Simultaneous detection of tumor markers in lung cancer using scanning electrochemical microscopy

Xin Ning, Qiang Xiong, Fan Zhang*, Pingang He

College of Chemistry and Molecular Engineering, East China Normal University, 500 Dongchuan Road, Shanghai 200241, PR China

ARTICLE INFO

ABSTRACT

Cancer became a global public health problem and one of the most causes of death, and early diagnosis will decrease mortality and extend lifespan of patients. In this study, the simultaneous detection of four tumor markers in lung cancer (alpha-fetoprotein (AFP), carcinoembryonic antigen (CEA), neuron-specific enolase (NSE), cytokeratin-19-fragment (Cyfra21-1)) was achieved for the first time using immune sandwich structures coupled with generation collection (GC) mode of scanning electrochemical microscopy (SECM). The proposed method exhibited excellent performance in quantitative detection of the four target proteins. A good linear correlation between the signal current issued from reduction of p-benzoquinone (BQ) oxidized from hydroquinone (H_2Q) and the amount of target tumor markers at logarithmic protein concentrations ranging from 5 ng/mL to 1 μg/mL was achieved. The detection limit was also low, meeting the needs of clinical use. The specificity was satisfactory and signal current of the target protein was unaffected by other simultaneously detected target proteins and common interfering species. Overall, the proposed method looks promising for high-throughput protein determination based on SECM, which could potentially be applied in clinical lung cancer diagnosis.

1. Introduction

Today, cancer became a global public health problem, threatening tens of millions of lives worldwide. Lung cancer ranks on top, with high patients mortality among all cancers [1]. The cancer screening and early diagnosis could efficiently improve patient survival rate and prolong lifespan. Thus, a number of methods have recently been integrated into immunoassays for cancer diagnosis, including electrochemical [2–5], photochemical [6–9], and chromatography [10–12].

Compared to other methods, electrochemical detection often exhibits elevated sensitivity but limited in multiple targets analysis. Since the electrochemical signals are generated by electro-active species, the overlap of multiple signals of target species with those from interferences makes the analysis difficult [13]. In clinical diagnosis, the combined determination of multiple tumor markers in presence of interferences is important to reduce the probability of false-positive results and improve the accuracy of diagnosis. Therefore, the development of methods allowing the simultaneous determination of multiple targets is essential.

Scanning electrochemical microscopy (SECM), invented by Allen J. Bard in the 1980s [14], has shown a great potential in this area [15]. SECM employs ultramicroelectrodes (UMEs) that can be moved over a substrate to record changes in faradaic current, depending on both the topography and the electrochemical activity of the substrate. Thus, SECM achieves the separation between the signal receiver (UMEs, also known as a tip) and carrier (substrate), enabling the simultaneous determination of multiple targets immobilized on the substrate in the well-designed area after successive scans thanks to its advantages, SECM has been exploited for the simultaneous determination of multiple DNA and proteins [16–21]. In this regard, we have been pioneers in developing biosensing platforms for the simultaneous determination of nine target DNAs using microarray with high sensitivity [22]. However, for protein biosensing, only two different proteins associated with atrophic gastritis and gastric cancer have yet been detected simultaneously using SECM [23], which deemed insufficient in clinical use. Therefore, the simultaneous detection of multiple tumor markers becomes crucial in achieving more accurate diagnosis.

In this study, the simultaneous detection of four tumor markers in lung cancer was achieved for the first time using SECM and sandwich-structured immune recognition. Note that alpha-fetoprotein (AFP) and carcinoembryonic antigen (CEA) are broad-spectrum tumor markers highly expressed in many cancers [24,25], and neuron-specific enolase (NSE) and cytokeratin-19-fragment (Cyfra21-1) are specific to lung cancer [26,27]. It has been reported that combined detection of broad spectrum and specific tumor markers can increase accuracy of cancer diagnosis [28,29]. The antibodies corresponding to the four tumor

---
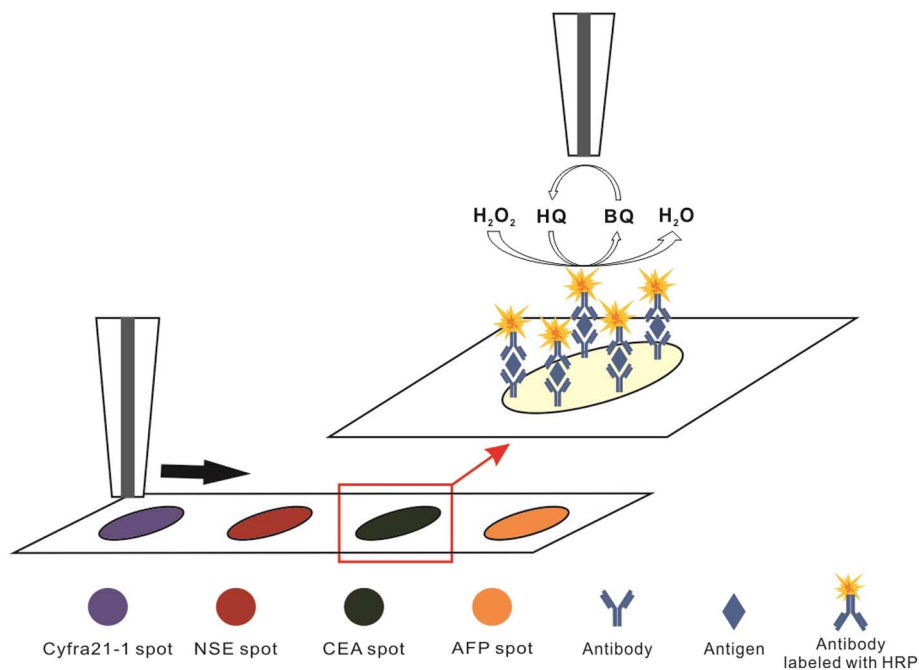
Scheme 1. A schematic representation of immune sandwich structures and signal generation on the protein microarray.

markers were firstly immobilized on the substrate to form protein microarrays. The addition of target proteins yielded sandwiched structures using horseradish peroxidase (HRP) modified antibodies (Scheme 1). In the presence of H_2O_2, HRP catalyzed the oxidation of hydroquinone (H_2Q) to form benzoquinone (BQ) on the spots. The generated BQ was, in turn, reduced by the tip upon potential polarization to yield satisfactory signal currents.

2. Material and methods

2.1. Materials

NaH_2PO_4, Na_2HPO_4, KCl, hydroquinone (H_2Q) and benzoquinone (BQ) were purchased from Sinopharm Chemical Reagent Co., Ltd., and bovine serum albumin (BSA) from Sangon Biotech (Shanghai, China) Co., Ltd. Target proteins (AFP, CEA, NSE, Cyfra21-1) and their respective antibodies (mouse anti-human AFP, mouse anti-human CEA, mouse anti-human Cyfra21-1, mouse anti-human NSE) were obtained from ChengHao Biosystems, Shanghai. Triton X-100 and thrombin were from Sigma, and ferrocenemethanol (FAM) were from Tokyo Chemical Industry (TCI). The biochips with four spots of antibodies corresponding to four target proteins were supplied by Shanghai Biotechnology Co., Ltd. (Shanghai, China). All solutions were prepared with ultrapure water obtained by a Millipore Milli-Q water purification system.

2.2. Construction of immune sandwich structures

The microarrays of immune sandwich structures were deposited on the biochips at room temperature. The biochip modified with four antibodies, including mouse anti-human AFP, CEA, Cyfra21-1 and NSE, was first rinsed with 1% Triton and then treated with 1% BSA for 1 h to block the nonspecific binding sites. Afterward, the biochip was immersed in target protein solutions at different concentrations for 2 h, followed by rinsing with the PBS solution. Next, the biochip was immersed in 5 μg/mL antibodies solution for another 1 h, forming the

immune sandwich structures. Finally, the unbound antibodies were washed away by PBS solution and the bioships were stored at room temperature.

2.3. SECM measurements

The SECM measurements were performed with a CHI 920C scanning electrochemical microscope (CH Instruments, Austin, TX, USA) at room temperature. The SECM set-up consisted of a piezo positioner, a controller that can move the tip in three dimensions, and a bipotentiostat. A typical three-electrode configuration was used: amperometric SECM tip Pt microelectrode (25 μm in diameter) as working electrode, an Ag/AgCl (3 M KCl) as a reference electrode, and a Pt wire as counter electrode. As we previously reported [22], the addition of 0.1% Triton X-100 prevented the passivation of the tip during detection, thus limiting the adsorption of generated redox species. The above-prepared biochip was used as a substrate during the SECM measurements. Z-approaching curves and SECM images were obtained with substrate generation/tip collection (SG/TC) mode of SECM in 0.1 M PBS (pH 7.4) containing 1 mM H_2Q, 1 mM H_2O_2, and 0.1% Triton X-100.

3. Results and discussion

3.1. Optimization of experimental conditions for SECM measurements

To obtain the optimal tip potential held during SECM measurements, cyclic voltammetry curves were recorded in 0.1 M PBS containing 1 mM BQ using a 25 μm Pt microelectrode as the tip. Fig. 1A showed the classic S-shaped curve of the microelectrode. At more negative potentials than −0.2 V, the current changed more slowly. Hereby, −0.4 V was selected as the tip potential for SECM measurements.

The approaching curves were acquired using the selected potential on the spot with and without target protein, and the results are gathered in Fig. 1B. The presence of target protein caused the formation of immune sandwich structures, linking HRP to the spot. HRP could
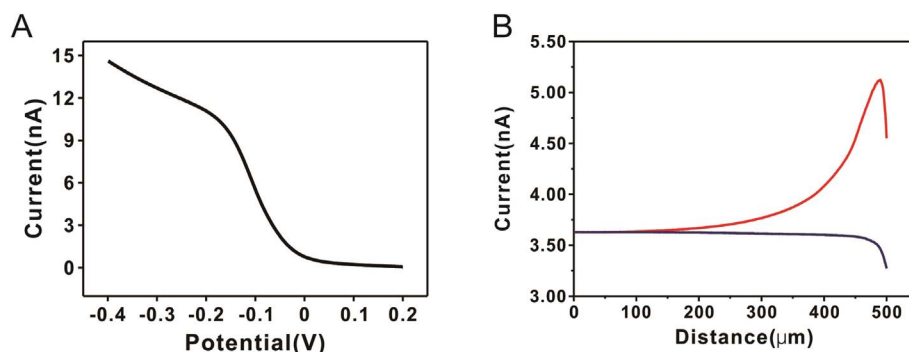
Fig. 1. (A) Cyclic voltammogram of 1 mM BQ in 0.1 M PBS solution containing 0.1% Triton (pH = 7.4). (B) The approaching curves above the spot with (red) and without (blue) target protein. (For interpretation of the references to color in this figure legend, the reader is referred to the web version of this article.)
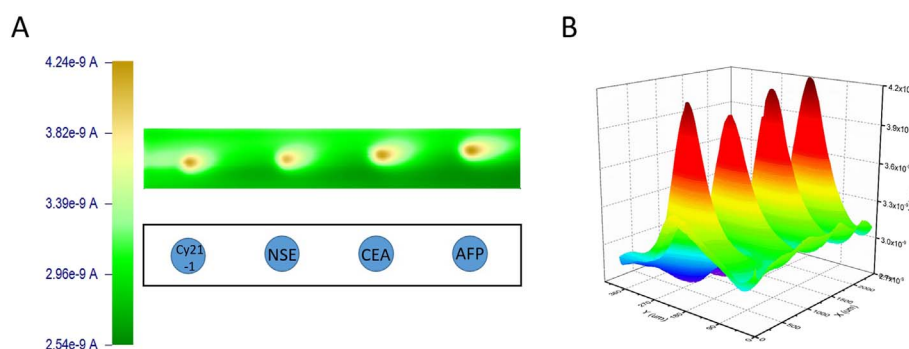

Fig. 2. (A) SECM imaging of four target proteins with the same concentration (1 μg/mL). (B) Corresponding 3D image. The diameter of the tip is 10 μm and scan rate is 5 μm/s.

oxidize H_2Q to BQ in presence of H_2O_2. The diffusion of the generated BQ increased its concentration near the spot, generating stronger reduction current signal as the tip approached the spot. When the tip was extremely close to the spot, the limited space blocked the diffusion of BQ to the tip, and the reduction current rapidly dropped (red curve). The maximum value appeared at about 10 μm from the tip to spot. Thus, a distance of 10 μm was selected for subsequent imaging. By contrast, the absence of target protein led to unfeasible oxidation of H_2Q, and no reduction current was detected by the tip while approaching the spot (blue curve).

3.2. SECM imaging of protein microarray

Using the optimal tip potential and distance between the tip and substrate, SECM imaging of protein microarray was performed. Before scanning, the substrate required horizontal adjustment to maintain a constant distance between the tip and chip [22]. As illustrated in Fig. 2,
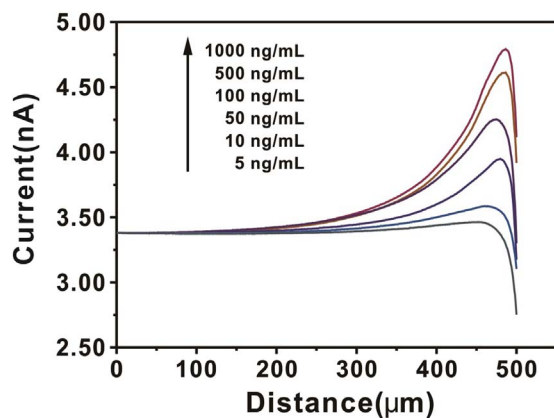

Fig. 3. Approaching curves of CEA at different concentrations ranging from 5 ng/mL to 1 μg/mL.

the four spots were all lightened and distinguishable, indicating that respective incubations with these target proteins generated positive feedback signals without signal overlap with those from interferences. Four target proteins were simultaneously detected using one redox couple without complicated design or operation, exhibiting the potential in high-throughput detection.

3.3. Quantitative measurement of target proteins

The correlation between the concentration of target proteins and tip current was investigated using the approaching curves. As shown in Fig. 3, the tip current enhanced as target proteins concentrations rose. This could drive HRP in larger amounts to reach the spot, leading to more BQ reduced by the tip upon polarization. The approaching curves also showed that when the tip was relatively far away from the spot, small and steady background currents were generated, probably produced by reduction of some oxidizing substances present in the solution.

To achieve quantitative analysis with high accuracy, signal current (ΔI) was determined, defined as the difference in peak current at about 15 μm over the spot and background current. Obviously, all target proteins displayed excellent linear correlations between signal current and logarithm of the concentrations from 5 ng/mL to 1 μg/mL (Fig. 4). The corresponding linear equations and correlation coefficients are presented in Table 1. The determination sensitivities are satisfactory, and the detection limits are much lower than the reference values displayed in Table 2 [30,31]. These values could be used for cancer screening. In other words, it might be confirmed cases if the detection values are higher than these reference values. The comparisons reveal the feasibility of the proposed method in clinic analysis.

3.4. Specificity of protein microarray

To evaluate the specificity of the proposed protein microarray, the biochip with the immobilization of four antibodies was incubated with
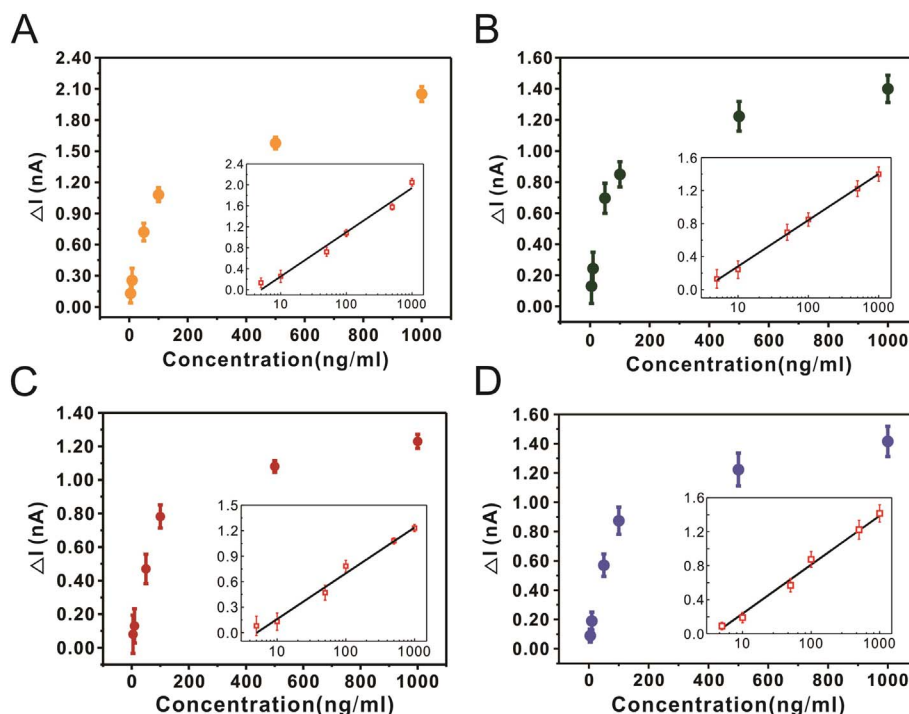
Fig. 4. Correlation curves between signal current (ΔI) and concentration of four target proteins: (A) AFP, (B) CEA, (C) NSE, and (D) Cyfra21-1. The inner diagram shows the linear correlations between signal current and logarithmic concentration of the four target proteins.

Table 1
Linear equations and correlation coefficients of four target proteins.

Target protein	Liner equation	Correlation coefficient
AFP	$\Delta I_{AFP} = 0.844 \times lgC_{AFP} - 0.593$	0.977
CEA	$\Delta I_{CEA} = 0.560 \times lgC_{CEA} - 0.278$	0.999
Cyfra21-1	$\Delta I_{Cy21-1} = 0.575 \times lgC_{Cy21-1} - 0.339$	0.987
NSE	$\Delta I_{NSE} = 0.539 \times lgC_{NSE} - 0.379$	0.969

Table 2
Comparison between reference values and detection limits of four target proteins recorded in this study.

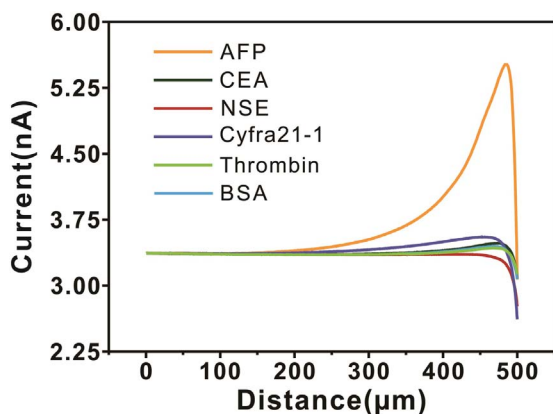|	Reference value	Detection limit
AFP	7.2 ng/mL	0.40 ng/mL
CEA	7.4 ng/mL	0.42 ng/mL
Cyfra21-1	3.3 ng/mL	0.67 ng/mL
NSE	12.5 ng/mL	0.69 ng/mL

Fig. 5. Approaching curves of 1 µg/mL AFP and other five interfering proteins at concentrations of 1 mg/mL.

six proteins, including AFP, CEA, NSE, Cyfra21-1, thrombin and BSA, respectively, followed by the SECM scanning. Fig. 5 gathers the approaching curves on AFP spot in presence of six proteins (1 mg/mL), respectively. Obviously, only AFP exhibited a positive feedback whereas the others showed no distinct positive feedbacks, although their concentrations are 1000 times higher than that of AFP. This was further demonstrated by comparing the signal currents in Fig. 6A. The other three spots displayed similar results, indicating that the four target proteins did not interfere with each other and were not influenced by other common proteins. The excellent specificity of the constructed protein microarray allowed the simultaneous detection of the proteins without interferences.

4. Conclusions

Four tumor markers in lung cancer were simultaneously detected for the first time using SECM of constructed immune sandwich structures. Under the optimized tip potential and distance between the tip and substrate, the signal currents of target proteins were correlated to the logarithm of concentrations from 5 ng/mL–1 µg/mL with good linearity. The determination sensitivities were substantial coupled with low detection limit. Moreover, protein microarray displayed excellent specificity towards other simultaneously detected target proteins and common interfering proteins. Overall, the proposed method shows promising future in clinical lung cancer diagnosis and high-throughput determination.

Urgency statement

Urgent publication is justified by the wonderful exhibition of simultaneous detection of four tumor markers related to lung cancer based on scanning electrochemical microscopy. The strategy suggested in this work meets the needs of clinical diagnosis and is respected to show promising future in multiobjective and high-throughput determination using scanning electrochemical microscopy.
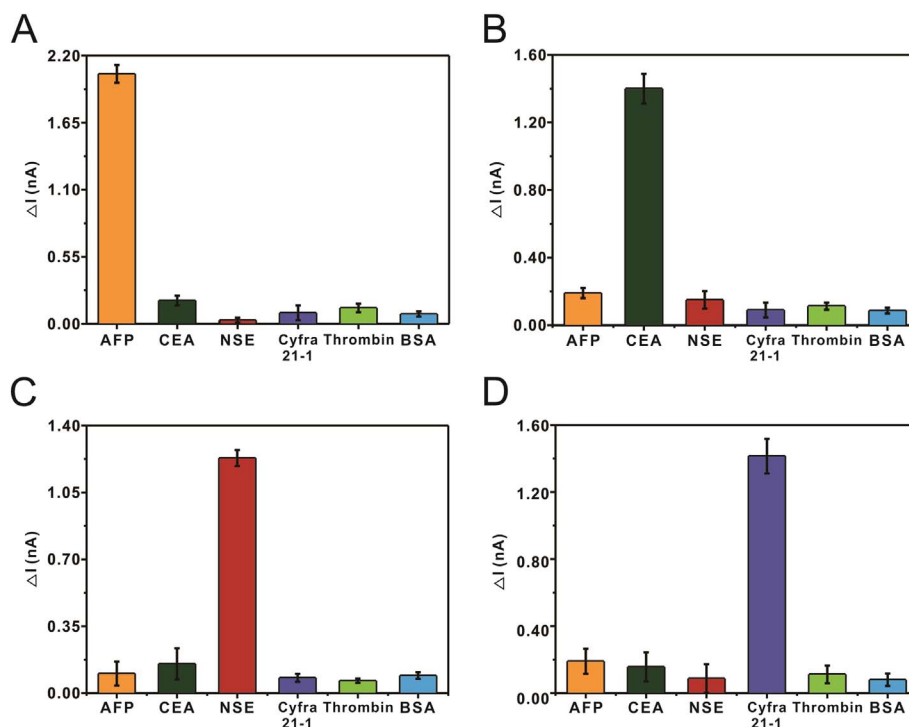
Fig. 6. Signal currents of the target and interfering proteins obtained from the spots with (A) AFP, (B) CEA, (C) NSE and (D) Cyfra21-1 as target proteins, respectively.

Acknowledgements

References

[1] L.A. Torre, F. Bray, R.L. Siegel, J. Ferlay, J. Lortet-Tieulent, A. Jemal, Global cancer statistics, 2012, CA Cancer J. Clin. 65 (2015) 87–108.

[2] S. Viswanathan, C. Rani, A. Vijay Anand, J.A. Ho, Disposable electrochemical immunosensor for carcinoembryonic antigen using ferrocene liposomes and MWCNT screen-printed electrode, Biosens. Bioelectron. 24 (2009) 1984–1989.

[3] D. Lin, J. Wu, F. Yan, S. Deng, H. Ju, Ultrasensitive immunoassay of protein biomarker based on electrochemiluminescent quenching of quantum dots by hemin bio-bar-coded nanoparticle tags, Anal. Chem. 83 (2011) 5214–5221.

[4] D. Lin, J. Wu, M. Wang, F. Yan, H. Ju, Triple signal amplification of graphene film, polybead carried gold nanoparticles as tracing tag and silver deposition for ultrasensitive electrochemical immunosensing, Anal. Chem. 84 (2012) 3662–3668.

[5] D. Tang, R. Yuan, Y. Chai, Ultrasensitive electrochemical immunosensor for clinical immunoassay using thionine-doped magnetic gold nanospheres as labels and horseradish peroxidase as enhancer, Anal. Chem. 80 (2008) 1582–1588.

[6] W. Tu, W. Wang, J. Lei, S. Deng, H. Ju, Chemiluminescence excited photoelectrochemistry using graphene-quantum dots nanocomposite for biosensing, Chem. Commun. 48 (2012) 6535–6537.

[7] C. Zong, J. Wu, C. Wang, H. Ju, F. Yan, Chemiluminescence imaging immunoassay of multiple tumor markers for cancer screening, Anal. Chem. 84 (2012) 2410–2415.

[8] C. Zong, J. Wu, M. Liu, F. Yan, H. Ju, High-throughput imaging assay of multiple proteins via target-induced DNA assembly and cleavage, Chem. Sci. 6 (2015) 2602–2607.

[9] S.J. Xiao, P.P. Hu, X.D. Wu, Y.L. Zou, L.Q. Chen, L. Peng, J. Ling, S.J. Zhen, L. Zhan, Y.F. Li, Sensitive discrimination and detection of prion disease-associated isoform with a dual-aptamer strategy by developing a sandwich structure of magnetic microparticles and quantum dots, Anal. Chem. 82 (2010) 9736.

[10] E. Vidal, M. Marquez, A.J. Raeber, K. Meissner, B. Oesch, M. Pumarola, Applicability of a rapid chromatographic immunoassay for analysis of the distribution of PrPBSE in confirmed BSE cases, Vet. J. 177 (2008) 448–451.

[11] A.H. Tasbiti, A. Bahrmand, M.A. Shokrgozar, M. Ghanei, A. Fateh, A. Karimi, S. Yari, Evaluation of antigen detection test (chromatographic immunoassay): potential to replace the antibody assay using purified 45-kDa protein for rapid diagnosis of tuberculosis, J. Clin. Lab. Anal. 28 (2014) 70–76.

[12] A. Martin, D. Bombeeck, K. Fissette, P. de Rijk, I. Hernandez-Neuta, P. Del Portillo, J.C. Palomino, Evaluation of the BD MGIT TBc Identification Test (TBc ID), a rapid chromatographic immunoassay for the detection of Mycobacterium tuberculosis complex from liquid culture, J. Microbiol. Methods 84 (2011) 255–257.

[13] A. Bardea, E. Katz, I. Willner, Probing antigen–antibody interactions on electrode supports by the biocatalyzed precipitation of an insoluble product, Electroanalysis 12 (2015) 1097–1106.

[14] J. Kwak, A.J. Bard, Scanning electrochemical microscopy. Theory of the feedback mode, Anal. Chem. 61 (1989) 1221–1227.

[15] D. Polcari, P. Dauphin-Ducharme, J. Mauzeroll, Scanning electrochemical microscopy: a comprehensive review of experimental parameters from 1989 to 2015, Chem. Rev. 116 (2016) 13234–13278.

[16] Z. Zhang, J. Zhou, A. Tang, Z. Wu, G. Shen, R. Yu, Scanning electrochemical microscopy assay of DNA based on hairpin probe and enzymatic amplification biosensor, Biosens. Bioelectron. 25 (2010) 1953–1957.

[17] W.S. Roberts, F. Davis, J.L. Holmes, S.D. Collyer, L.D. Larcombe, S.L. Morgan, S.P. Higson, Detection and imaging the expression of the trans-membrane protein CD44 in RT112 cells by use of enzyme-labeled antibodies and SECM, Biosens. Bioelectron. 41 (2013) 282–288.

[18] W. Song, Z. Yan, K. Hu, Electrochemical immunoassay for CD10 antigen using scanning electrochemical microscopy, Biosens. Bioelectron. 38 (2012) 425–429.

[19] A.J. W, F. Zhou, Scanning electrochemical microscopy imaging of DNA microarrays using methylene blue as a redox-active intercalator, Langmuir the Acs Journal of Surfaces & Colloids 24 (2008) 5155–5160.

[20] A.A. Gorodetsky, W.J. Hammond, M.G. Hill, K. Slowinski, J.K. Barton, Scanning electrochemical microscopy of DNA monolayers modified with nile blue, Langmuir the Acs Journal of Surfaces & Colloids 24 (2008) 14282–14288.

[21] B. Liu, A.J. Bard, C.Z. Li, H.B. Kraatz, Scanning electrochemical microscopy. 51. Studies of self-assembled monolayers of DNA in the absence and presence of metal ions, J. Phys. Chem. B 109 (2005) 5193–5198.

[22] H. Fan, X. Wang, F. Jiao, F. Zhang, Q. Wang, P. He, Y. Fang, Scanning electrochemical microscopy of DNA hybridization on DNA microarrays enhanced by HRP-modified SiO_2 nanoparticles, Anal. Chem. 85 (2013) 6511–6517.

[23] T. Yasukawa, Y. Hirano, N. Motochi, H. Shiku, T. Matsue, Enzyme immunosensing of pepsinogens 1 and 2 by scanning electrochemical microscopy, Biosens. Bioelectron. 22 (2007) 3099–3104.

[24] X.-F. Wang, Y.-H. Wu, M.-S. Wang, Y.-S. Wang, CEA, AFP, CA125, CA153 and CA199 in malignant pleural effusions predict the cause, Asian Pac. J. Cancer Prev. 15 (2014) 363–368.

[25] C.Z. He, K.H. Zhang, Q. Li, X.H. Liu, H. Yan, N.H. Lv, Combined use of AFP, CEA, CA125 and CAl9-9 improves the sensitivity for the diagnosis of gastric cancer, BMC Gastroenterol. 13 (2013) 1–5.

[26] R. Molina, X. Filella, J.M. Augé, R. Fuentes, I. Bover, J. Rifa, V. Moreno, E. Canals, N. Viñolas, A. Marquez, Tumor markers (CEA, CA 125, CYFRA 21-1, SCC and NSE) in patients with non-small cell lung cancer as an aid in histological diagnosis and prognosis, Lung Cancer 24 (2003) 209–218.

[27] J. Schneider, H.G. Velcovsky, H. Morr, N. Katz, K. Neu, E. Eigenbrodt, Comparison

of the tumor markers tumor M2-PK, CEA, CYFRA 21-1, NSE and SCC in the diagnosis of lung cancer, Anticancer Res. 20 (2000) 5053.

[28] S. Tsuboi, K. Taketa, K. Nouso, T. Fujikawa, K. Manabe, H. Ohmori, T. Higashi, Y. Shiratori, High level of expression of alpha-fetoprotein receptor in gastric cancers, Tumor Biol. 27 (2006) 283–288.

[29] S. Ishigami, S. Natsugoe, H. Nakashima, K. Tokuda, A. Nakajo, H. Okumura, M. Matsumoto, S. Nakashima, S. Hokita, T. Aikou, Biological aggressiveness of alpha-fetoprotein (AFP)-positive gastric cancer, Hepato-Gastroenterology 53 (2006)

338.

[30] A.V.D. Gaast, C.H. Schoenmakers, T.C. Kok, B.G. Blijenberg, F. Cornillie, T.A. Splinter, Evaluation of a new tumour marker in patients with non-small-cell lung cancer: Cyfra 21.1, Br. J. Cancer 69 (1994) 525–528.

[31] J. Järvisalo, M. Hakama, P. Knekt, U.H. Stenman, A. Leino, L. Teppo, J. Maatela, A. Aromaa, Serum tumor markers CEA, CA 50, TATI, and NSE in lung cancer screening, Cancer 71 (1993) 1982–1988.